Journal of Metals, Materials and Minerals, 34(3), 2033, 2024

Investigating the oxidation behavior of Mg-Zn alloy: Effects of heating rates, gas flow, protective atmosphere, and alloy composition

Tuğçe Nur SARAÇOĞLU[1], Safa POLAT[2,3], Erkan KOÇ[1], Muwafaq MASHRA[2,3], Amir NAJAH SAUD[1,4,*], and Marta MICHALSKA-DOMAŃSKA[5]

[1] *Biomedical Engineering, Karabuk University, Turkey*
[2] *Material Research and Development Laboratory, Karabuk University, Turkey*
[3] *Metallurgy and Materials Engineering, Karabuk University, Turkey*
[4] *Biomedical Engineering, Al-Mustaqbal University College, Babylon, Iraq*
[5] *Institute of Optoelectronics, Military University of Technology, 2 Kaliskiego Str., 00-908 Warsaw, Poland*

***Corresponding author e-mail**: amir.saud92@gmail.com

Received date:
21 April 2024
Revised date:
6 June 2024
Accepted date:
25 June 2024

Keywords:
Magnesium alloys;
Mg-Zn alloy;
Casting;
DTA-Tg analysis;
High temperature oxidation

Abstract

Magnesium-zinc alloys offer promising lightweight properties but are prone to oxidation during high-temperature processing and usage. In this study, the oxidation behavior of Mg-Zn alloy was examined according to the inert gas type flow rate, heating rate and alloy amount. Initially, alloys were produced by adding zinc at weight percentages of 0.5%, 1.5%, and 2% using the casting method. The alloys were characterized using X-ray fluorescence (XRF), X-ray Diffraction (XRD), and scanning electron microscope (SEM) analyses, revealing the formation of dendritic Mg-Zn intermetallic within the alloy. The oxidation behavior of these alloys was examined via differential thermal analysis (DTA) and thermogravimetric analysis (TGA), considering factors such as heating rate, gas flow rate, type of protective atmosphere, and amount of alloying element. The results indicated that the onset temperature of oxidation decreased with increasing heating rate. The effect of gas flow rate varied depending on the heating rate and the type of gas. Under a nitrogen atmosphere, conditions with a heating rate of 20°C·min^{-1} and a gas flow rate of 5 cm^3·min^{-1} resulted in the least oxidation. In an argon atmosphere, a gas flow rate of 5 cm^3·min^{-1} was found to be sufficient to prevent oxidation. However, at a gas flow rate of 1 cm^3·min^{-1}, a heating rate of 20°C·min^{-1} was more effective in preventing oxidation. The alloying element (zinc) likely reduced oxidation, particularly at the 1.5% addition level, possibly due to the formation of intermetallic compounds.

1. Introduction

Magnesium alloys, renowned for their low density and high strength-to-weight ratio compared to steel and aluminum, are highly desirable for a wide array of applications in the aerospace, defense, and automotive industries [1-5]. They are significantly more ductile and easier to process compared to resin-based plastic composites [6-9]. However, these alloys are also flammable and can be difficult to weld, which can limit their use in certain applications [10]. Additionally, it is well-established that the ability of magnesium and its alloys to resist oxidation diminishes notably at temperatures exceeding 400°C [11,12]. Magnesium alloys are also prone to surface damage and may even combust when exposed to elevated temperatures in the presence of air during processes like casting, welding, and heat treating [13,14]. This degradation occurs because of the reaction of magnesium with oxygen at high temperatures, leading to the formation of the MgO layer on the surface, followed by cracking of this layer due to the vaporization of Mg in the interior.

Until now, the general aim has been either to reduce the oxidation rate of magnesium by incorporating certain alloying elements or to strengthen the oxide layer formed on the surface by using the oxides of alloying elements. In this context, Qiyang *et al*. aimed to increase the oxidation resistance of Mg-9Al-1Zn alloy at high temperatures by alloying it with Be and Ca [10]. Their investigation revealed that the combination of Be and Ca facilitated the formation of a composite layer consisting of CaO and MgO on the surface of the alloy. This composite layer effectively mitigated Mg evaporation and hindered the advancement of oxidation into the inner regions. Dong *et al.* examined the oxidation characteristics of the AZ31 magnesium alloy by incorporating Ca and CaO within the temperature range of 450 to 650°C [15]. Their findings indicated that the inclusion of CaO eased the dissolution of Ca into the matrix, leading to the formation of Al_2Ca. Consequently, this formation mitigated the combustion and oxidation of the molten Mg, thereby reducing the necessity for using harmful SF_6 gas during casting. Luoyi Wu and Zhong Yang conducted a study on the high-temperature oxidation behavior of the Mg-2.1Gd-1.1Y-0.82Zn

alloy utilizing thermogravimetric analysis [16]. Their observations revealed an increase in mass due to oxidation as temperature rose, accompanied by rapid surface oxidation until a protective oxide layer developed. Subsequently, they noted the formation of intermittent macroscopic defects. However, they noted that the presence of Gd and Y alloying elements hindered the entry of oxygen into the alloy upon oxidation, thereby impeding further oxidation after the formation of a thin oxide film. Xiaowen Yu and colleagues explored the high-temperature oxidation behavior of the Mg-Y alloy by introducing Zn to the Mg-3Y alloy and conducting tests in a dry-air environment at temperatures ranging from 500°C to 530°C [17]. The findings revealed the formation of Y_2O_3 and MgO layers on the alloy surface. Additionally, they observed that the incorporation of Zn facilitated the formation of Y_2O_3; however, when the Zn content exceeded 2.5%, the formation of ZnO increased. Consequently, this resulted in the degradation of the surface oxidation film and a reduction in the alloy's oxidation resistance. Changchang Liu *et al.* investigated the oxidation behavior of three magnesium alloys (AZ31, WE43, and ZE10) in air, subjecting them to varying heating rates (5, 10, 15, and 20°C·min^{-1}) from a different perspective. Their findings revealed that ZE10 exhibited a higher mass gain compared to AZ31 and WE43, with increments of 17% and 18%, respectively [18]. Considering all these studies, it can be concluded that while the effectiveness of SF_6 gas has been extensively investigated, the impact of less harmful gases such as nitrogen and argon has not been thoroughly examined. Furthermore, the literature lacks sufficient information regarding the effects of heating rate and commonly used alloying elements such as zinc under these conditions.

To address this gap, magnesium alloys containing pure zinc and different ratios of zinc were initially produced by casting method. The resulting products were characterized using XRD, XRF, and SEM analyses. Subsequently, DTA-TG analyses were performed under different heating rates and gas flow rates of nitrogen and argon. In these analyses, heating-holding and cooling steps were followed to determine the stage and conditions of oxidation. Furthermore, after these analyses, macro and micro (SEM) images of the samples were taken to interpret the formation and progression of oxidation on the surface. As a result, based on the obtained findings, the conditions and alloys with the least oxidation were identified, and comparisons were made with the literature.

2. Experimental methods

2.1 Raw materials

Magnesium and zinc metals, each with a purity of 99%, were utilized in the experiments. Both argon and nitrogen gases, with a purity of 99%, were employed for inerting purposes. Casting was carried out using AISI1040 quality steel, while aluminum oxide crucibles were selected for thermal analysis. These materials were chosen for their high purity levels, aiming to ensure the reliability of the experimental study.

2.2 Mg-Zn alloy preparation

The melting and casting of magnesium alloys were conducted using a specially designed electrical resistance furnace capable of withstanding temperatures of up to 1100°C. Illustrated in Figure 1(a), the furnace comprises a thermocouple (1), Ar input (2), ceramic plug (3), Ar circulation indicator (4), Ar output (5), crucible (6), resistor (7), and fireproof components (8). To initiate alloy production, magnesium and zinc metals were placed within a 2 kg capacity graphite crucible, which was then positioned within the furnace. Heating commenced with the target temperature set at the melting point of 750°C. Throughout the heating process, argon gas was introduced into the environment to prevent oxidation. Approximately 60 min were required to achieve the desired processing temperature and complete melting of the metals within the crucible. Meanwhile, molds crafted from AISI1040 steel, depicted in Figure 1(b), were heated to 250°C in an ash furnace and prepared for casting. Subsequently, the molds were positioned beneath the crucible, and the molten metal was poured into them by opening a hole at the bottom of the crucible to facilitate flow, thus enabling the casting process. Following solidification of the liquid metal within the molds, a cooling period of approximately 30 min was allowed. Subsequently, the molds were opened, and the alloy samples were retrieved, marking the completion of the alloy production process.

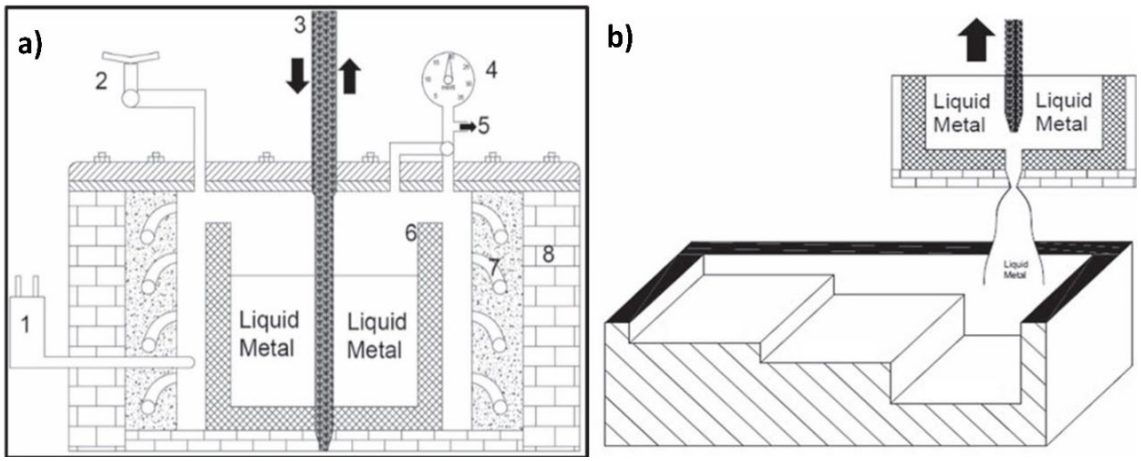

Figure 1. (a) Melting furnace schematic details (1-Thermocouple, 2-Arinput, 3-Ceramicstopple, 4 Arcirculationindicator, 5-Aroutput, 6-Meltingpot, 7-Resistance, 8-Refractory) and (b) casting schematic details.

2.3 Characterization methods

The chemical compositions of the prepared Mg alloys were determined utilizing a Rigaku Primus II-WD-XRF spectrometer, which was equipped with a 4-kW rhodium tube. For crystal structure analysis within the range of 15° to 90°, the Rigaku Ultima IV X-ray diffraction (XRD) device, featuring a Cu-based X-ray source and a fixed monochromator at 40 kV and 40 mA, was employed. For microstructural analysis, the samples were first subjected to metallographic preparation processes, as in our previous studies. The samples were ground with SiC papers (180 to 2000 grain sizes) in parallel lines at a 90° angle, then cleaned with deionized water, polished with a 0.3 μm alumina solution, and rinsed with ethanol [19-21]. Finally, the samples were etched with a picryl solution (picric acid, acetic acid, distilled water, and ethanol) to reveal the microstructure [22]. Following this process, the microstructure of each sample was examined using a Carl Zeiss ULTRA PLUS scanning electron microscope (SEM). The chemical compositions of the observed phases were assessed via energy dispersion spectroscopy (EDS) integrated into the SEM.

2.4 DTA-TGA analysis

The oxidation behavior of the casting samples was examined using the differential scanning calorimetry (DTA) and thermogravimetric analyzer (TGA) STA7300 as given in our previous study [23]. For this purpose, the samples were subjected to a heating program starting at room temperature up to 700°C, followed by a 10 min holding time at this temperature and then cooled to 200°C for solidification [24]. First, pure magnesium samples were analyzed separately in N_2 and Ar inert gas environments, with gas flow rates of 1 cm^3 to 5 cm^3 and heating rates of 5, 10, and 20°C·min^{-1} using the heating program mentioned above. Based on the results, the same analyzes were performed for the alloys under conditions of 1 and 5 cm^3 gas flow rates, a heating rate of 20°C·min^{-1} and in an argon atmosphere only. The results obtained under these parameters were first presented graphically. Subsequently, based on these plots, the extent and oxidation states were determined for each sample as a function of heating rate and gas flow rate. In addition, the results were correlated with macroscopic and SEM of the sample surfaces.

3. Results

3.1 Material characterization

The chemical composition of the samples, comprising pure magnesium and Mg-xZn alloys (where x=0.5%, 1.5%, 2%), was initially determined via XRF analysis by measuring at least three different parts of each sample. The measurement uncertainty of these compositions is 1%. As depicted in Table 1, the results indicated that the observed zinc content in the alloys closely matched the intended ratios of added Zn. However, it was observed that the Zn content in the Mg-2Zn alloy slightly deviated from the target value of 2 wt%. This deviation could be attributed to incomplete homogenization of the mixture during the casting process. Additionally, trace amounts of other elements were detected in these alloys, likely stemming from impurities in the raw materials. However, it has been also observed that it contains around 2% oxygen.

The phase analyses of magnesium and its alloys were conducted using XRD as depicted in Figure 2(a). The findings revealed the presence of characteristic peaks corresponding to the (100), (002), (101), (102), (110), (103), (112), (201), and (004) planes of alpha-magnesium (α-Mg) at approximately 32°, 34°, 36°, 47°, 57°, 63°, 68°, 69°, and 72° for the 2θ values (JCPDS No. 35-0821) [25]. In the pure Mg sample, the XRD pattern shows distinct peaks corresponding to the hexagonal close-packed (hcp) structure of magnesium, with prominent peaks at (100), (002), (101), and other characteristic planes. For the Mg-0.5Zn alloy, the pattern is like pure Mg but with slight shifts and additional peaks. The diffraction peaks for Mg are present with minor intensity changes, suggesting that Zn is present in solid solution and possibly forming minor secondary phases.

In the Mg-1.5Zn alloy, more significant changes are observed in the diffraction peaks. The Mg peaks are present, but additional peaks appear, indicating the formation of Zn-rich phases or intermetallic compounds. The Mg-2Zn alloy shows pronounced changes with additional peaks. The peaks corresponding to Mg are still present but reduced in intensity, and new peaks indicate the formation of Mg-Zn intermetallic compounds. In the XRD range of 35° to 38° for pure Mg, a sharp peak is observed at around 36° corresponding to the (101) plane of Mg. In the Mg-2Zn alloy, this peak is shifted and broadened, indicating the presence of Zn. There is also an additional peak around 37°, which can be attributed to the formation of Mg-Zn intermetallic compounds or solid solution effects. However, in the graph provided in Figure 2(b), peak splitting is observed in the Mg-2Zn sample compared to pure Mg. While part of this splitting originates from the (100) plane of Mg, another part may arise from either the (002) plane of Zn (ID: 00-001-1238) or the Mg-Zn (ID: 04-007-1412) intermetallic compound [26-28]. Furthermore, there are slight shifts observed in many planes, notably in the (101) plane of Mg, which are likely attributed to the formation of secondary phases and solid precipitates [29].

Table 1 The average elemental compositions of the composites (±0.01).

Alloy	Weight % Chemical Composition				
	Zn	Al	Si	Mn	Mg
Pure Mg	0.01	-	0.04	-	Balance
Mg-0,5Zn	0.53	0.04	-	-	
Mg-1,5Zn	1.55	0.05	-	0.02	
Mg-2Zn	1.87	-	0.03	-	

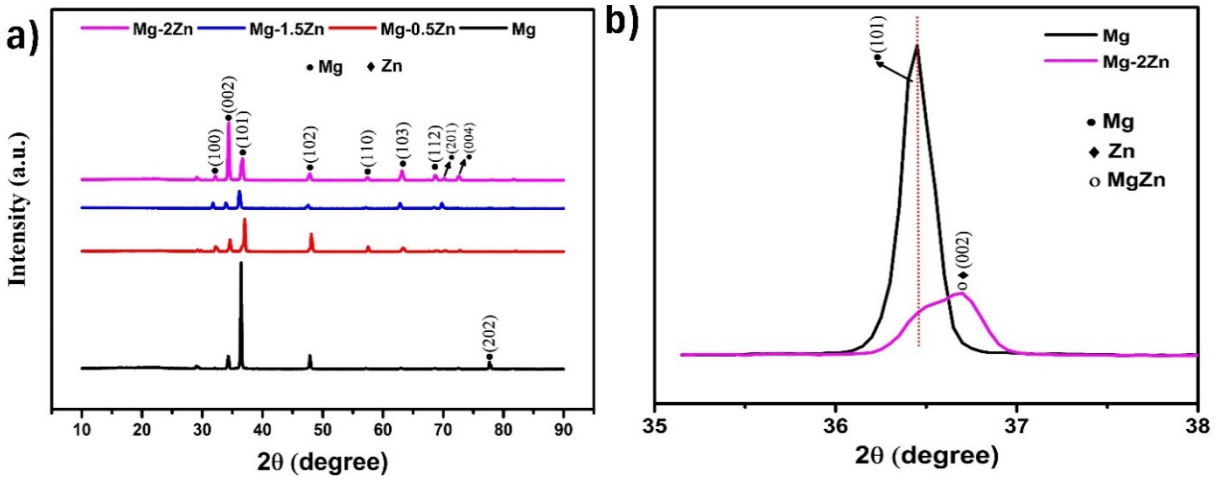

Figure 2. (a) XRD analysis results of pure magnesium and its alloys, and (b) the range of 35-38° for Mg and Mg-2Zn.

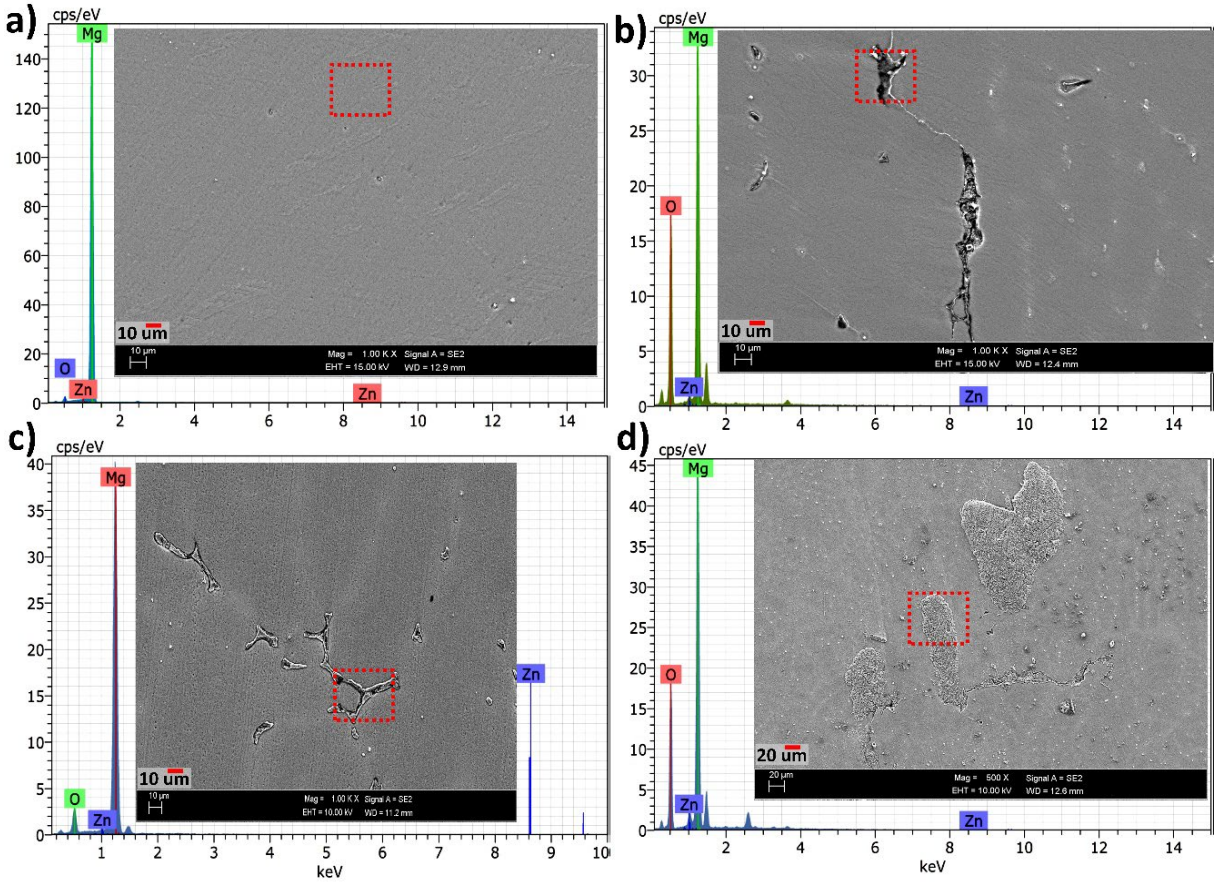

Figure 3. SEM images of samples with EDX (a) Mg, (b) Mg-0.5Zn, (c) Mg-1.5Zn, and (d) Mg-2Zn.

The formation of solid solutions and intermetallic compounds can account for the variations in diffraction peaks. The addition of Zn to Mg can lead to the formation of a solid solution [30,31], where Zn atoms substitute Mg atoms in the hcp lattice, causing lattice distortion and slight shifts in the diffraction peaks caused by different atomic diameters [32,33]. The Zn atoms in the Mg-0.5Zn alloy are probably dissolved in the Mg matrix, which results in small shifts in the Mg diffraction peaks and marginal variations in peak intensities. At higher Zn concentrations, such as in the Mg-1.5Zn and Mg-2Zn alloys, the formation of intermetallic compounds (e.g., Mg-Zn) is more likely. Certain compounds form additional diffraction peaks and have unique crystal structures. Increased lattice strain from the higher Zn content, the formation of multiple phases, and grain size reduction are the causes of the broadening of peaks and changes in intensity, particularly seen in the Mg-2Zn alloy.

Figure 3 shows the microstructure images of pure magnesium and its alloys as well as the corresponding EDX spectra. It shows that the morphology of Mg-Zn phase gradually changes from punctate to flake with increasing Zn content. This indicates that the Zn content increases significantly in the second phase, where Zn is mainly present,

and a small amount is dissolved in the Mg matrix. As the Zn content increases, the probability that the second phase will form increases.

These results show that the EDX spectrum in the pure magnesium sample (Figure 3(a)) has a dominant magnesium peak with no significant peaks for Zn or other elements, indicating a homogeneous magnesium matrix. The surface appears relatively smooth and has few features. The surface of the Mg-0.5Zn sample (Figure 3(b)) shows distinctive features, such as crack-like structures. The EDX spectrum shows a prominent peak for Mg and smaller peaks for Zn and O. This indicates the possible oxidation or contamination of Zn as well as its low presence. Due to the higher Zn content, the Mg-1.5Zn sample (Figure 3(c)) has more prominent features or precipitates, including a larger Zn peak in the EDX spectrum. This suggests that Zn-rich phases or precipitates are forming, and that oxidation may be occurring. For larger agglomerations or precipitations, the Mg-2Zn sample (Figure 3(d)) exhibits even more complex features. The EDX spectrum shows a strong Mg peak, a significant Zn peak and a notable O peak. This indicates that significant phase separation or precipitate formation can occur at higher Zn concentrations, with oxidation most likely occurring at the surfaces or boundaries of the precipitates. These observations and studies from the literature show that the formation of secondary phases or precipitates in magnesium alloys is a direct consequence of increasing the Zn content. According to the literature, Zn strengthens magnesium alloys by forming intermetallic compounds such as magnesium-zinc, which improve mechanical properties such as hardness and tensile strength [34]. Studies have shown that Mg alloys are susceptible to oxidation, particularly at grain boundaries or precipitation interfaces where Zn-rich phases can form [35,36]. The oxidation observed in these SEM images is consistent with these results. Furthermore, the microstructural characteristics depicted in these images align with existing literature findings. Specifically, studies showed that the addition of zinc (Zn) leads to increasingly intricate and pronounced microstructures as its concentration rises.

3.2 Oxidation characterization

3.2.1 Nitrogen atmosphere for pure magnesium

To determine the oxidation characteristics, the behavior of pure magnesium in nitrogen and argon atmospheres was first examined, followed by the behavior of Zn alloy samples in an argon atmosphere. The parameters of heating rate, gas flow rate, and gas type were examined in these analyses. For this purpose, investigations began with pure magnesium, utilizing nitrogen as a protective atmosphere. Additionally, these analyses were programmed into heating, holding, and cooling stages. The expected observations of oxidation, melting, and solidification in each graph are denoted by abbreviations: "OX" for oxidation, "ME" for melting, and "SO" for solidification.

According to the analysis results in Figure 4 under nitrogen atmosphere, at a heating rate of 5°C·min^{-1}, oxidation began before melting in both gas flow rates (1 cm^3 and 5 cm^3), with a partial melting peak observed. Immediately after melting, oxidation was also observed, and no peak was observed during holding and cooling. At the same time, there is likely an approximately 40% increase in mass attributed to this oxidation in the TGA graph of this analysis (Figure 4(f)). At a heating rate of 10°C·min^{-1}, oxidation is relatively less pronounced before melting, but it is predominantly observed during the holding period (Figure 4(c)). Furthermore, no significant effect of heating rates has been observed here. Additionally, the mass increases attributed to these oxidations have also occurred at around 40% (Figure 4(d)). At a heating rate of 20°C·min^{-1}, oxidation was observed both before and after melting, as well as during the holding period, in the 1 cm^3 gas flow (Figure 4(a)). However, no solidification was observed. In the 5 cm^3 gas flow, only a small amount of oxidation occurred after melting, with no significant oxidation observed otherwise. Notably, solidification was observed for the first time in the 5 cm^3 gas flow, likely due to the reduced occurrence of oxidation. Additionally, the mass increase observed in the TGA analysis was approximately 15%, which is notably lower compared to the others, indicating reduced oxidation (Figure 4(b)).

3.2.2 Argon atmosphere for pure magnesium

The analysis results of pure magnesium conducted in an argon atmosphere are presented in Figure 5. According to these results, both melting, and solidification peaks were clearly observed at a heating rate of 5°C·min^{-1} and a gas flow rate of 5 cm^3 (Figure 5(e)), with nearly less than 10% oxidation occurring (Figure 5(f)). However, at 15 cm^3 gas flow rate, oxidation occurred before melting (Figure 5(c)), resulting in a mass increase of around 40% (Figure 5(d)). Similarly, at heating rates of 10°C·min^{-1} and 20°C·min^{-1} (Figure 5(a) and Figure 5(c)), oxidation occurred before melting at 15 cm^3, while it was observed to be less than 10% at 55 cm^3 (Figure 5(b) and Figure 5(d)). Among these conditions, the least oxidation, approximately 3%, occurred at a heating rate of 20°C·min^{-1} and 5 cm^3 argon gas flow (Figure 5(b)). Additionally, when the heating rate was increased to 20°C·min^{-1}, the onset of oxidation at 15 cm^3 approached the melting peak, and the amount of oxidation decreased compared to the other conditions.

Based on these results, it can be said that the protective atmosphere of argon gas reduces oxidation independently of the heating rate as the gas flow rate increases. This is likely due to argon gas replacing oxygen molecules in the reaction environment and limiting magnesium's reaction with the atmosphere [18]. This is an expected phenomenon commonly encountered in the literature. However, the decrease in oxidation with increasing heating rate is an unexpected result because, at high temperatures, molecular mobility generally increases, which can accelerate reaction rates and lead to combustion or ignition [37]. Here, at low heating rates, magnesium is likely exposed to heat for a longer period and absorbs more heat, as evidenced by the DTA graphs. This probably increases oxidation efficiency by allowing magnesium to react even with the smallest amount of oxygen in the environment before melting, even with a gas flow rate of 55 cm^3. Therefore, it is considered necessary to increase the heating rate before melting along with the gas flow rate to reduce oxidation in an argon atmosphere.

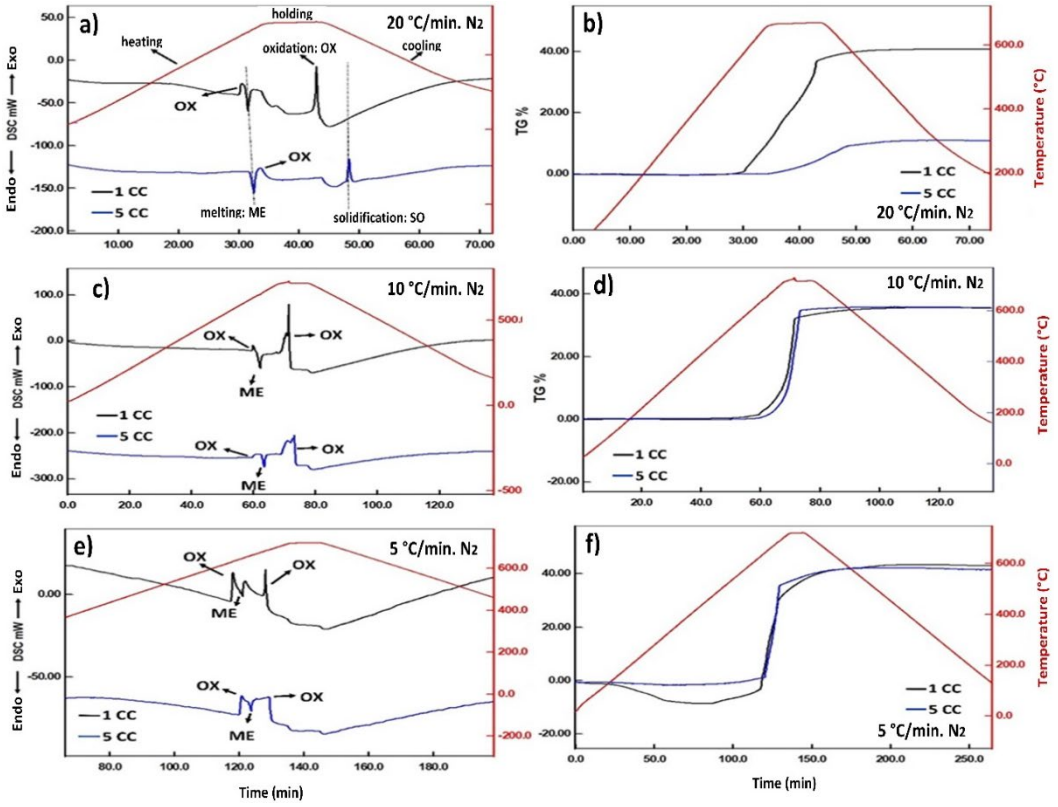

Figure 4. DTA and Tg analysis of pure magnesium in a nitrogen gas atmosphere (a-b) 20°C·min^{-1}, (c-d) 10°C·min^{-1}, and (e-f) 5°C·min^{-1}

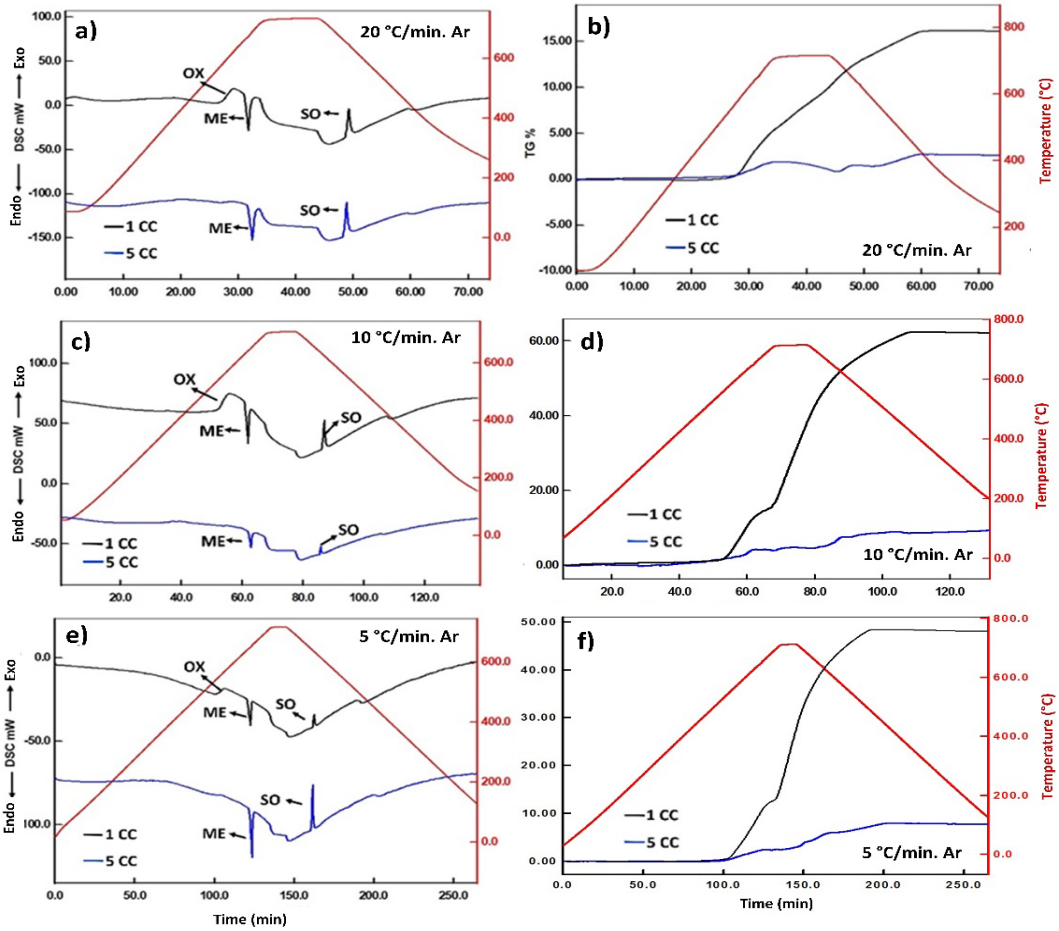

Figure 5. DTA and Tg analysis of pure magnesium in argon gas atmosphere (a-b) 20°C·min^{-1} , (c-d) 10°C·min^{-1}, and (e-f) 5°C·min^{-1}.

3.3 Argon atmosphere for alloys

The analysis results for Mg-Zn alloys in an argon atmosphere are presented in Figure 6. In these analyses, the heating rate was kept constant at 10°C·min^{-1}, while the gas flow rate (argon) was applied at 1 cm^3 and 5 cm^3, with zinc element added to magnesium alloy at weight percentages of 0.5%, 1.5%, and 2%. In almost all these analyses, melting and solidification peaks were clearly observed. Additionally, the least oxidation (less than 10%) was observed in all samples at a gas flow rate of 5 cm^3, which is consistent with previous analyses. However, at a gas flow rate of 1 cm^3, oxidation occurred before melting, as observed in others. Nevertheless, regardless of sample and gas flow rate, an oxidation peak after solidification was observed, which was not observed in others and is likely attributed to the zinc alloy element. It is thought that this peak is related not only to oxidation but also to the solidification of zinc in the alloy. According to these results, it is evident that the addition of zinc reduces oxidation up to a certain point. There are several possible reasons for this decrease in oxidation with zinc addition. Primarily, magnesium alloys with added zinc are more stable, and this stability may prevent oxygen from diffusing into the magnesium [38]. Another reason could be that zinc has a lower affinity for oxygen compared to magnesium. Alternatively, zinc might form a protective oxide layer on the surface, preventing further oxidation [39]. These factors seem to be effective at a zinc content of 1.5%, but not at 0.5%. At a zinc content of 2%, it is likely that zinc itself starts to oxidize, diminishing its effectiveness. When it comes to gas flow rate, during heating, magnesium's affinity for oxygen increases, causing it to react even with small amounts of oxygen present [40]. However, increasing the gas flow rate reduces the presence of oxygen in the environment, which likely leads to the observed reduction in oxidation during the experiments.

In Figure 7, microstructure images along with the results of EDX analysis after DTA analysis of alloys in 1 cm^3 are presented. According to these results, the regions indicated in the red square, which are likely to be MgO, are thought to be ignitions on the surface [41]. These are probably the parts of magnesium in contact with oxygen. In some regions, there are zinc contents, and it is thought that ZnO has formed in these regions [42]. However, these formations are considered to have occurred without much brightness compared to MgO formations. This is because MgO ignitions rapidly react on surfaces, forming very fine geometrically white formations [42]. It is observed that these brightnesses occur less in samples with added zinc. The reason for this is probably that zinc reacts with magnesium to form an intermetallic compound and reduces magnesium's affinity for oxygen [42]. With the addition of 1.5% Zn, this formation probably occurred quite efficiently, as less brightness is observed in the visuals compared to others (Figure 7(c)). However, when the zinc content is 2%, it is thought that the affinity of zinc for oxygen also increases, and it tries to contribute to oxidation. Because, as seen in Figure 7(e) and f, it is observed that zinc-containing regions are also oxidized but do not show brightness.

.

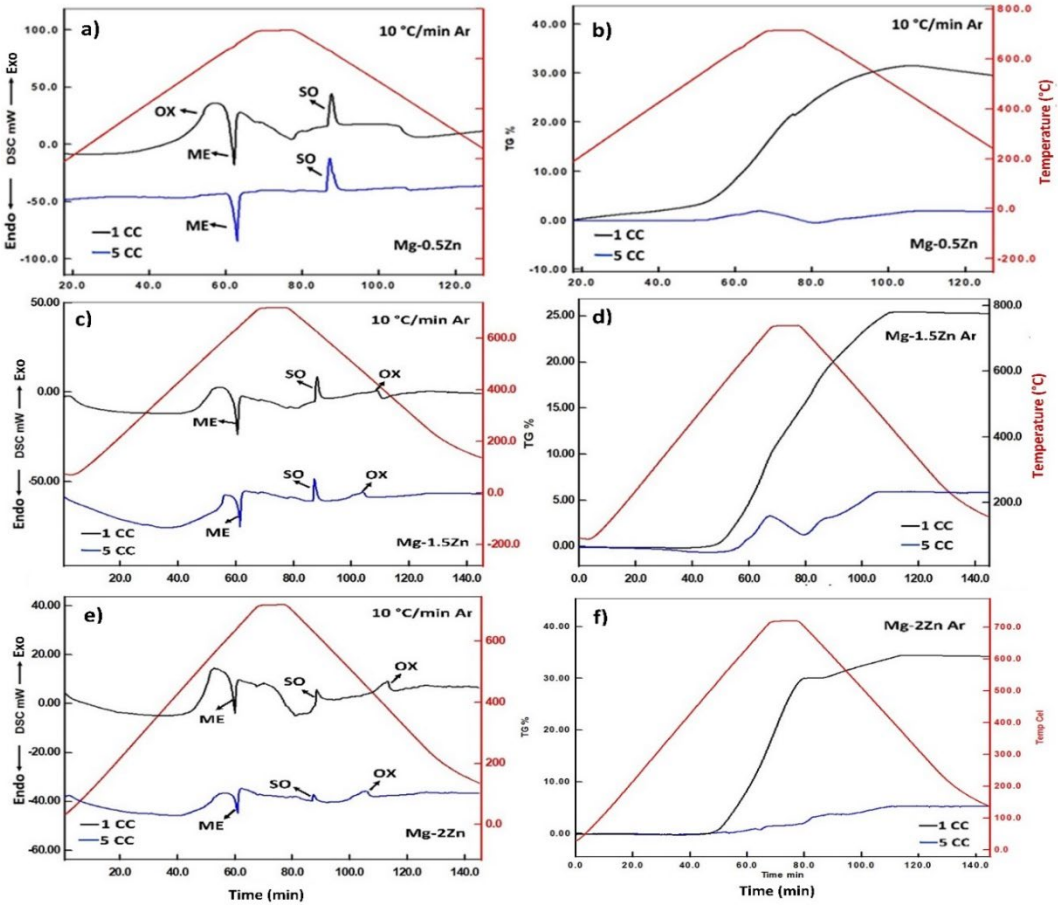

Figure 6. DTA and Tg analysis of (a-b) Mg-0.5Zn, (c-d) Mg-1.5Zn, and (e-f) Mg-2Zn.

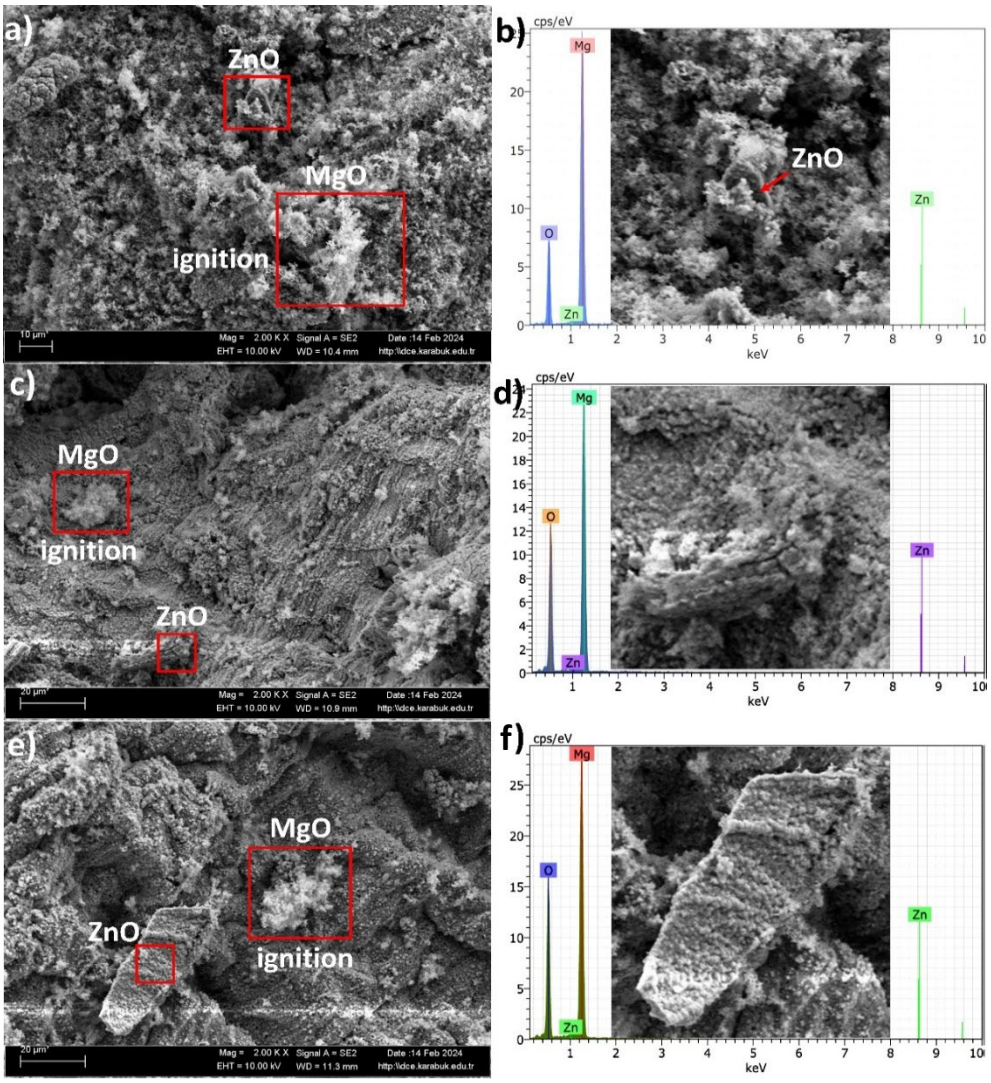

Figure 7. SEM Images of Samples After DTA Analysis with EDX (a-b) 0.5% Zn, (c-d) 1.5% Zn, and (e-f) 2% Zn.

Table 3. Effect of Alloying Additions on Oxide Phases Formed during Oxidation of Magnesium-Based Alloys [43].

Alloys composition	Gas flow	Heating rate	Ignition temperature	Oxide phases	References
Mg-Ca-Al	Air	11.6°C·min^{-1}	700°C	MgO, CaO, $Ca(OH)_2$, Al_2O_3	[44]
Mg-Ca-Y				MgO, CaO, Y_2O_3	
Mg-Ca	Air	7.3°C·min^{-1} to 9.1°C·min^{-1}	440°C to550°C	MgO, CaO	[45]
AZ91-*x*Ca	Air	2.5°C·min^{-1}	Up to 700°C	MgO, CaO	[46]
AZ91-*x*Ca-*y*Y				MgO, CaO, Y_2O_3	
Mg-*x*Y-Zn-*y*Zr	Air	0.025°C·min^{-1}	400°C	MgO, Y_2O_3	[47]
Mg-8Al-0.1RE	Air	10°C·min^{-1}	700°C	MgO, RE_2O_3, Al_2O_3	[48]
Mg-9Al-1Zn	Air	1.5°C·min^{-1}	400°C to 450°C	MgO, CaO, BeO	[10]
AZ31-0.3Ca	Air	5°C·min^{-1}	450°C to 650°C	MgO, CaO	[15]
AZ31-0.3CaO					
I. Mg-3Y-*x*Zn	Air	4.16°C·min^{-1} to 1.41°C·min^{-1}	500°C to 530°C	MgO, Y_2O_3, ZnO	[17]
I. IAZ31	Air	5°C·min^{-1} to 20°C·min^{-1}	1000°C	MgO oxide	[18]
III. ZE10					
IV. WE43					
V. Mg-9Al-1Zn-*x*Be	Air	1.33°C·min^{-1} 0.046°C·min^{-1}	400°C	MgO MgO, BeO	[42]
VI. Pure Mg	N_2	20°C·dk^{-1}	~660°C	Probably MgO, ZnO	This study
VII. Pure Mg	Ar	20°C·dk^{-1}	~630°C	Probably MgO, ZnO	
VIII. Pure Mg	Ar	10°C·dk^{-1}	~570°C	Probably MgO, ZnO	
VIII. Mg-Zn	N_2	20°C·dk^{-1}	~660°C	Probably MgO, ZnO	

In addition, a summary of studies conducted in the literature from the past to the present has been made, and the results are given in Table 3. According to the results in this table, it is understood that calcium is the alloying element that increases the ignition temperature of magnesium the most (around 700°C). Then, aluminum and zinc can be said to follow (approximately 500°C). These analyses were observed when dry air was used. In our study, nitrogen and argon were initially used for pure magnesium. Results showed that the least oxidation occurred at a heating rate of 20°C·min^{-1} and a gas flow rate of 5 cm^3 during nitrogen usage, with ignitions present at around 650°C. Furthermore, significant oxidation was observed at almost every heating rate in the analysis of pure magnesium with argon gas at a 1 cm^3 gas flow rate. The onset of oxidation approached the melting point as the heating rate increased. For instance, at a heating rate of 20°C·min^{-1}, possible ignitions in 1 cm^3 occurred around 620°C. When the alloying element (Zn) was added, it is presumed that oxidation occurred after solidification at a gas flow rate of 5 cm^3 and a heating rate of 10°C·min^{-1}, with ignition occurring around (approximately 670°C). At a 1 cm^3 gas flow rate, ignition likely occurred before melting. The removal of oxygen from the environment by nitrogen and argon gases is a significant factor here. Another factor is the heating rate; for a reactive metal like magnesium, a high heating rate before melting is quite effective in reducing oxidation. Finally, it is believed that zinc, as an alloying element, probably reduces the oxidation of magnesium by forming intermetallic compounds up to a certain level. However, beyond a certain level, its own oxidation negatively affects the process

4. Conclusion

In this study, the oxidation behavior of magnesium-zinc alloys was investigated. For this purpose, alloys were first produced by adding 0.5 wt%, 1.5 wt%, and 2 wt% zinc using the casting method. The produced alloys were characterized using XRF, XRD, and SEM analyses, revealing the formation of dendritic Mg-Zn intermetallic within the alloy. The oxidation behavior of these alloys was examined using DTA analysis, considering factors such as heating rate, gas flow rate, type of protective atmosphere, and amount of alloying element. According to the results obtained, it was observed that the onset temperature of oxidation decreases as the heating rate increases. The effect of gas flow rate was found to vary depending on the heating rate and the type of gas. Under nitrogen atmosphere, conditions with a heating rate of 20°C·min^{-1} and a gas flow rate of 5 cm^3·min^{-1} resulted in the least oxidation. In argon atmosphere, a gas flow rate of 5 cm^3·min^{-1} was found to be sufficient to prevent oxidation regardless of the heating rate. However, at a gas flow rate of 1 cm^3·min^{-1}, a heating rate of 20°C·min^{-1} was more effective in preventing oxidation. The alloying element (Zn) likely reduced oxidation, particularly at the addition level of 1.5%, possibly due to the formation of intermetallic compounds.

Acknowledgments

This study was conducted at the Materials Research and Development Laboratories of Karabuk University (MARGEM). We would like to thank the entire team that facilitated the use of the laboratory facilities.

Declaration of competing interest

The authors declare that they have no known competing financial interests or personal relationships that could have appeared to influence the work reported in this paper.

References

[1] I. Polmear, D. StJohn, J-F. Nie, and M. Qian, "Light alloys: Metallurgy of the light metals," Butterworth-Heinemann; 2017.

[2] S. K. Aldriasawi, N. H. Ameen, K. I. Fadheel, A. M. Anead, H. E. Mhabes, and B. Mohamad, "An Experimental artificial neural network model: Investigating and predicting effects of quenching process on residual stresses of AISI 1035 steel alloy n.d.

[3] S. Polat, Y. Sun, E. Çevik, and H. Colijn, "Evaluation of thermal conductivity of GNPs-doped B4C/Al-Si composites in terms of interface interaction and electron mobility," *Diamond and Related Materials*, vol. 98, p. 107457, 2019.

[4] M. K. Kulekci, "Magnesium and its alloys applications in automotive industry," *The International Journal of Advanced Manufacturing Technology*, vol. 39, pp. 851-865, 2008.

[5] S. Polat, "Theoretical modeling and optimization of interface design to improve thermal conductivity in Mg-Dia composites," *Ceramics International*, vol. 48, pp. 4763-4774, 2022.

[6] B. Jiang, W. Liu, D. Qiu, M-X. Zhang, and F. Pan "Grain refinement of Ca addition in a twin-roll-cast Mg–3Al–1Zn alloy," *Materials Chemistry and Physics*, vol. 133, pp. 611-616, 2012.

[7] F. Pan, M. Yang, and X. Chen, "A review on casting magnesium alloys: Modification of commercial alloys and development of new alloys," Journal of Materials Science & Technology, vol. 32, pp. 1211-1221, 2016.

[8] A. Abdelhussein, G. Yang, E. K. Hussein, L. Li, and B. Mohamad, "Investigation of fracture behavior and mechanical properties of epoxy composites supported with MWCNTs microscopically," *Vibroengineering Procedia*, vol. 54, pp. 193-201, 2024.

[9] S. Polat, A. Avcı, and M. Ekrem, "Fatigue behavior of composite to aluminum single lap joints reinforced with graphene doped nylon 66 nanofibers," *Composite Structures*, vol. 194, pp. 624-632, 2018.

[10] Q. Tan, N. Mo, B. Jiang, F. Pan, A. Atrens, and M-X. Zhang "Combined influence of Be and Ca on improving the high-temperature oxidation resistance of the magnesium alloy Mg-9Al-1Zn," *Corrosion Science*, vol. 122, pp. 1-11, 2017.

[11] M. Liu, D. S. Shih, C. Parish, and A. Atrens, "The ignition temperature of Mg alloys WE43, AZ31 and AZ91," *Corrosion Science*, vol. 54, pp. 139-142, 2012.

[12] A. Atrens, G-L. Song, M. Liu, Z. Shi, and F. Cao, "Dargusch MS. review of recent developments in the field of magnesium corrosion," *Advanced Engineering Materials*, vol. 17, pp. 400-453, 2015.

[13] F. Czerwinski, "The oxidation behaviour of an AZ91D magnesium alloy at high temperatures," *Acta Materialia*, vol. 50, pp. 2639-2654, 2002.

[14] X. Yu, S. Shen, B. Jiang, Z. Jiang, H. Yang, and F. Pan "The effect of the existing state of Y on high temperature oxidation properties of magnesium alloys," *Applied Surface Science*, vol. 370, pp. 357-363, 2016.

[15] D. B. Lee, "High temperature oxidation of AZ31+0.3wt.%Ca and AZ31+0.3wt.%CaO magnesium alloys," *Corrosion Science,* vol. 70, pp. 243-251, 2013.

[16] L. Wu, and Z. Yang, "Oxidation behaviour of Mg–2.1Gd–1.1Y–0.82Zn–0.11Zr alloy at high temperatures," *Journal of Alloys and Compounds*, vol. 626, pp. 194-202, 2015.

[17] X. Yu, B. Jiang, J. He, B. Liu, Z. Jiang, and F. Pan, "Effect of Zn addition on the oxidation property of Mg-Y alloy at high temperatures," *Journal of Alloys and Compounds,* vol. 687, pp. 252-262, 2016.

[18] C. Liu, S. Lu, Y. Fu, and H. Zhang, "Flammability and the oxidation kinetics of the magnesium alloys AZ31, WE43, and ZE10," *Corrosion Science*, vol. 100, pp. 177-185, 2015.

[19] S. Polat, Y. Sun, and E. C\c evik, "Wear behavior of TiB2/GNPs and B4C/GNPs reinforced AA6061 matrix composites," *Journal of Tribology*, vol. 143, p. 111701, 2021.

[20] M. M. Karaca, S. Polat, and İ. Esen, "Reciprocating dry sliding wear behaviour of BN@MXene@AA7075 composites," *Journal of Composite Materials*, 00219983241257665, 2024.

[21] S. Polat, Y. Sun, E. Çevik, H. Colijn, and M. E. Turan, "Investigation of wear and corrosion behavior of graphene nanoplatelet-coated B_4C reinforced Al–Si matrix semi-ceramic hybrid composites," *Journal of Composite Materials*, vol. 53, pp. 3549-3565, 2019.

[22] E. Koç, A. Incesu, and A. N. Saud, "Comparative study on dry and bio-corrosive wear behavior of Mg-xAl-3Zn alloys (x = 0.5-1-2-3 wt.%)," *The Journal of Materials Engineering and Performance*, vol. 31, pp. 613-621, 2022.

[23] S. Polat, Y. Sun, E. Çevik, and H. Colijn, "Microstructure and synergistic reinforcing activity of GNPs-B4C dual-micro and nano supplements in Al-Si matrix composites," J*ournal of Alloys and Compounds*, vol. 806, pp. 1230-1241, 2019.

[24] A. W. Aldeen, D. Y. Mahdi, C. Zhongwei, I. A. Disher, and B. Mohamad, "Effect of isothermal and isochronal aging on the microstructure and precipitate evolution in beta-quenched N36 Zirconium alloy," *Facta Universitatis, Series: Mechanical Engineering*, 2023.

[25] N. Aboutalebianaraki, C. J. Neal, S. Seal, and M. Razavi "Bio-degradable Mg-Sc-Sr alloy improves osteogenesis and angiogenesis to accelerate bone defect restoration," *Journal of Functional Biomaterials*, vol. 13, p. 261, 2022.

[26] J. Kubásek, D. Dvorský, J. Šedý, Š. Msallamová, J. Levorová, R. Foltán, and D. Vojtěch, "The Fundamental comparison of Zn–2Mg and Mg–4Y–3RE alloys as a perspective biodegradable materials," *Materials*, vol. 12, p. 3745, 2019.

[27] F. Tong, X. Chen, Q. Wang, S. Wei, and W. Gao, "Hypoeutectic Mg-Zn binary alloys as anode materials for magnesium-air batteries," *Journal of Alloys and Compounds,* vol. 857, p. 157579, 2021.

[28] Y. Yan, X. Chu, X. Luo, X. Xu, Y. Zhang, Y. Dai, D. Li, L. Chen, T. Xiao, and K. yu, A homogenous microstructural Mg-based matrix model for orthopedic application with generating uniform and smooth corrosion product layer in Ringer's solution: Study on biodegradable behavior of Mg-Zn alloys prepared by powder metallurgy as a case," *Journal of Magnesium and Alloys*, vol. 9, pp. 225-240, 2021.

[29] S. Cai, T. Lei, N. Li, and F. Feng, "Effects of Zn on microstructure, mechanical properties and corrosion behavior of Mg–Zn alloys," *Materials Science and Engineering: C*, vol. 32, pp. 2570-2577, 2012.

[30] C. H. Caceres, G. E. Mann, and J. R. Griffiths, Grain size hardening in Mg and Mg-Zn solid solutions," *Metallurgical and Materials Transactions A,* vol. 42, pp. 1950-1959, 2011.

[31] P. K. Sahu, S. Pal, B. Das, and Q. Shi, "Fabrication and effect of Mg–Zn solid solution via Zn foil interlayer alloying in FSW process of magnesium alloy," *ArchivCivMechEng*, vol. 20, p. 137, 2020.

[32] H. Liu, F. Xue, J. Bai, J. Zhou, and X. Liu, "Effect of substitution of 1 at% Ni for Zn on the microstructure and mechanical properties of Mg94Y4Zn2 alloy," *Materials Science and Engineering: A*, vol. 585, pp. 387-395, 2013.

[33] L. R. Owen, and N. G. Jones, "Lattice distortions in high-entropy alloys," *Journal of Materials Research*, vol. 33, pp. 2954-2969, 2018.

[34] A. Javaid, and F. Czerwinski, "Effect of Zinc on solidification and aging behaviour of magnesium alloys containing rare earths" In: J. B. Jordon, V. Miller, V. V. Joshi, N. R. Neelameggham, Editors. Magnesium Technology 2020, Cham: Springer International Publishing; 2020, pp. 371-379.

[35] M. M. Castro, L. A. Montoro, A. Isaac, M. Kawasaki, and R. B. Figueiredo, "Mechanical mixing of Mg and Zn using high-pressure torsion," *Journal of Alloys and Compounds* vol. 869, p. 159302, 2021.

[36] F. Naghdi, and R. Mahmudi, "Effect of solution treatment on the microstructural evolution and mechanical properties of an aged Mg–4Zn–0.3Ca alloy," *Materials Science and Engineering: A*, vol. 631, pp. 144-152, 2015.

[37] Z. Meng, D. Yang, and Y. Yan, "Study of carbon black oxidation behavior under different heating rates," *The Journal of Thermal Analysis and Calorimetry,* vol. 118, pp. 551-559, 2014.

[38] E. Ghali, W. Dietzel, and K-U. Kainer, "General and localized corrosion of magnesium alloys: A critical review," *The Journal of Materials Engineering and Performance,* vol. 13, pp. 7-23, 2004.

[39] D. Lu, Y. Huang, J. Duan, and B. Hou, "A Zinc-rich coating fabricated on a magnesium alloy by oxide reduction," *Coatings*, vol. 9, p. 278, 2019.

[40] M. Malathi, K. M. Godiwalla, A. Kumar, E. Z. Chacko, S. K. Ajmani, and S. Ranganathan, "Generation of magnesium for in situ desulphurisation–investigations on influence of inert gas flowra," *Mineral Processing and Extractive Metallurgy*, vol. 123, pp. 67-74, 2014.

[41] C. Liu, S. Lu, Y. Fu, and H. Zhang, "Flammability and the oxidation kinetics of the magnesium alloys AZ31, WE43, and ZE10," *Corrosion Science*, vol. 100, 177-185, 2015.

[42] Q. Tan, N. Mo, B. Jiang, F. Pan, A. Atrens, and M-X. Zhang, "Oxidation resistance of Mg–9Al–1Zn alloys micro-alloyed with Be," *Scripta Materialia*, vol. 115, 38-41, 2016.

[43] F. Czerwinski, "The reactive element effect on high-temperature oxidation of magnesium," *International Materials Reviews*, vol. 60, 264-296, 2015.

[44] B. S. You, M. H. Kim, and W. W. Park, Chung IS, "Effect of Al and Y additions on the oxidation behavior of Mg-Ca base molten alloys," *Materials Science Forum*, vol. 419-422, 581-586, 2003.

[45] B-S. You, W-W. Park, and I-S. Chung, "The Effect of calcium addition to magnesium on the microstructure and compositional changes of oxide film formed at high temperature," *Materials Transactions,* vol. 42, 1139-1141, 2001.

[46] S. Cheng, G. Yang, J. Fan, Y. Li, and Y Zhou, "Effect of Ca and Y additions on oxidation behavior of AZ91 alloy at elevated temperatures," *Transactions of Nonferrous Metals Society of China*, vol. 19, pp. 299-304, 2009.

[47] Z. Ning, W. Liang, F. Cao, and J. Sun, "The effect of y on the oxidation of Mg-Zn-Zr alloys," *The International Journal of Modern Physics B,* vol. 23, pp. 796-801, 2009.

[48] J. Rao, and H. Li, "Oxidation and ignition behavior of a magnesium alloy containing rare earth elements," *The International Journal of Advanced Manufacturing Technology*, vol. 51, pp. 225-231, 2010.